$DyPO_4$: A Three-Dimensional Ising Antiferromagnet

J. C. Wright*† and H. W. Moos†
Department of Physics, The Johns Hopkins University, Baltimore, Maryland 21218

and

J. H. Colwell, B. W. Mangum, and D. D. Thornton‡
Heat Division, National Bureau of Standards, Washington, D. C. 20234

(Received 30 June 1970)

The magnetic susceptibility, heat capacity, and optical-absorption spectrum of $DyPO_4$ have been measured as a function of temperature and magnetic field. The optical-absorption spectrum indicates that the magnetic interactions in $DyPO_4$ have the form of the Ising interaction and occur primarily between nearest neighbors. The magnetic-susceptibility and heat-capacity measurements have been compared with exact series expansions for a diamond lattice assuming an Ising system with nearest-neighbor interactions. The theoretical calculations are in agreement with the measurements. The nature of the divergence of the heat capacity at the critical point is examined. Our data do not permit us to distinguish between the applicability of the logarithmic and power-law divergencies since they are indistinguishable in the region of our measurements. The temperature dependence of the critical field for the metamagnetic phase transition has also been determined and compared with the calculated value for the critical field at 0 K obtained from the spectroscopic measurements.

I. INTRODUCTION

The Ising model has received considerable attention because its idealized properties result in many theoretical simplifications. Investigations of the thermodynamic properties of this model have been made for various lattices in one, two, and three dimensions. Since analytic solutions exist only for the one-dimensional and some two-dimensional systems, the method of exact series expansions has been used to study a number of other lattices in two and three dimensions.[1] This method is one in which truncated exact expansions give successive approximations in the derivation of the physical quantities of interest such as the energy, magnetic susceptibility, magnetization, and heat capacity. The low-temperature series expansions for the diamond lattice, appropriate for $DyPO_4$, converge right up to the critical point,[2] unlike those for the other three-dimensional lattices.

In the past, the primary use of the Ising model of magnetic systems was that of a simple model for theoretical investigations of collective phenomena or for testing the reliability of various approximations to more physical models. Recently, a number of systems have been found that have primarily Ising interactions.[3–18] A detailed comparison of these systems with theory cannot generally be made, however, because of low crystal symmetry, the low ordering temperatures, or the presence of long-range interactions. In this paper, the results of magnetic-susceptibility, heat-capacity, and optical-spectra measurements on $DyPO_4$ are presented and compared with theoretical predictions. It is found that the heat-capacity and optical-spectra data are in excellent agreement with theoretical predictions. The magnetic-susceptibility measurements agree well with an exact series expansion for the energy, but they do not agree with a series expansion for the susceptibility. The reason for the disagreement is not known. It therefore appears that $DyPO_4$ may be a very good approximation to the three-dimensional Ising model for the diamond lattice.[19]

II. CRYSTAL STRUCTURE

$DyPO_4$ has the zircon crystal structure[20] which consists of linked DyO_4 and PO_4 tetrahedra (sharing oxygen atoms). The symmetry is tetragonal and there are four $DyPO_4$ molecules per unit cell. The

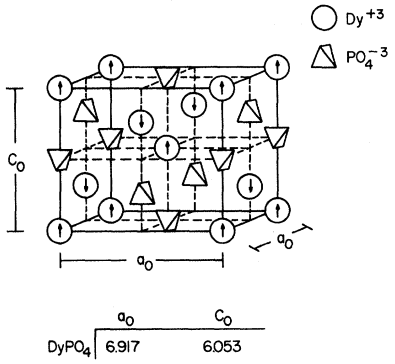

FIG. 1. Unit cell and lattice parameters of $DyPO_4$. The arrows in the circles indicate the ordered magnetic state of $DyPO_4$. The nearest neighbors of the central Dy^{3+} ion are the four Dy^{3+} ions lying on the faces of the unit cell.

space group is D_{4h}^{19} ($I4_1/amd$) and the unit-cell dimensions are $a_0 = 6.917$ Å and $c_0 = 6.053$ Å. The four magnetically equivalent Dy^{3+} ions per unit cell have a site symmetry D_{2d}. A given Dy^{3+} ion has four nearest neighbors 3.78 Å away which lie at the apexes of a flattened tetrahedron. In addition, there are four second-nearest neighbors at 5.71 Å and eight third-nearest neighbors at 5.75 Å. Figure 1 shows the arrangement of the magnetic ions in the lattice. The nearest neighbors of the central ion lie in the faces of the unit cell. The spin configuration of the ordered state has also been indicated in Fig. 1.

III. EXPERIMENTAL TECHNIQUES

A. Crystal Growth

Crystals of $DyPO_4$ were grown from a $Pb_2P_2O_7$ flux according to the method of Feigelson.[21] Crystals were typically about $0.3 \times 1 \times 4$ mm with the optic axis lying along the long direction. The crystals were generally of good optical quality and free of inclusions.

B. Heat Capacity

The $DyPO_4$ sample used in the heat-capacity experiments consisted of approximately 35 crystals weighing a total of 0.42 g. The sample was attached to a sample holder, which consisted of a thin copper sheet $25 \times 40 \times 0.25$ mm, by placing the sample on the holder and covering it with a drop of very dilute "low-temperature" varnish. The crystals were oriented on the holder such that for the measurements made in a magnetic field, the field would be along the c axis of the crystals. The thermal contact between the sample and the holder was very good. The thermal resistance determined in the transition region (the only region where the heating rates used were large enough to establish a discernible thermal lag) was of the order of 250 K/W. An encapsulated germanium resistance thermometer was attached to a small tab at one end of the sample holder by means of a threaded connector using a small amount of stopcock grease to enhance thermal contact. The calorimeter heater was varnished to the sides of the holder. This assembly was suspended in the inner jacket of a ^{3}He cryostat by fine nylon threads which passed through small holes in the corners of the copper holder. The sample was cooled by a mechanical heat switch[22] which made contact with a copper wire attached to the thermometer capsule. The heat-capacity measurements were made by the conventional discontinuous-heating method. Magnetic fields were applied to the sample by means of a superconducting solenoid which was wrapped on the outer vacuum jacket in the ^{4}He bath.

Two separate germanium thermometers were used in the heat-capacity measurements to cover different temperature ranges. Above 2.3 K a thermometer having a resistance of ~1000 Ω at 4.2 K was used, and it was calibrated against the National Bureau of Standards (NBS) provisional temperature scale No. 2-20 (1965),[23] utilizing 20 calibration points between 2.3 and 20 K. For measurements below 2.3 K, a thermometer having a resistance of ~150 Ω at 4.2 K was used. This thermometer was calibrated against the ^{3}He and ^{4}He vapor-pressure scales[24] and the calibration extended to 0.2 K using the magnetic temperature scale of cerous magnesium nitrate (CMN). The over-all uncertainty in the accuracy of the heat-capacity measurements below 4.2 K is approximately 1% except possibly at the lowest temperatures where it may be somewhat larger due to the smallness of the heat capacity and to uncertainties in the addenda correction. The accuracy of measurements below 4.2 K has been established by measurements using a standard copper sample. This procedure has not been followed in the region above 4.2 K and, hence, the accuracy of the measurements in that region may be lower due to unknown sources of systematic error, even though the precision of the measurements is better than 1%. The heat capacity of the addenda (sample holder, thermometer, etc.) was not measured directly, but was determined from the known amounts of the materials used and values derived from earlier experiments. This quantity is accurately known at lower temperatures and is approximately equivalent to 3.5 g of copper. Its contribution to the total heat capacity is only a few percent in the transition region but is comparable to the sample heat capacity below 1 K. A problem is encountered at higher temperatures because of the small amount of varnish, ~0.007 g, used to attach the sample to the holder, and a piece of Teflon tape, ~0.035 g, used to electrically insulate the heater leads. The heat capacity of these materials becomes a significant part of the total, but since the exact amount is uncertain the sample heat capacity cannot be accurately determined in the region above the transition. These heat capacities may be expected to vary as T^3 in the region of the measurements, as is expected to be the case for the lattice contribution to the sample heat capacity. Since for the purposes of the present paper we are only interested in the magnetic heat capacity, the magnitude of these T^3 contributions to the heat capacity have been determined from the high-temperature data and subtracted from the total heat capacity. The determination of the T^3 quantity is discussed below.

C. Magnetic Susceptibility

The parallel differential susceptibility of $DyPO_4$ was measured over the temperature range 0.3–20 K by the ac mutual-inductance method at a frequency

of 270 Hz. The sample (approximately 0.2 g) consisted of a number of relatively small single crystals (each having the shape of a parallelepiped) varnished together with the c axis of each crystal oriented parallel to the axis of the measuring coils. Subsequent measurements made with smaller coils on different samples, each consisting of one single crystal in the shape of a parallelepiped, gave the same results. Temperatures from 14 to 20 K were measured by comparing the vapor pressure above the pumped liquid H_2 with the tables of Barber and Horsford.[25] Below 4.2 K the temperature measurements were based on the 1958 ^{4}He scale of temperatures. A magnetic thermometer (chromic potassium alum), which had been calibrated against the vapor pressure of liquid ^{4}He pumped below the λ point, was used to measure temperatures in the range from 0.9 to 4.2 K. Thermal contact between sample and thermometer was achieved by a bundle of fine copper wires "potted" with the salt in Epoxy. Their free ends were tied on to the sample with thread and coated liberally with stopcock grease. From 0.3 to 1.0 K, temperatures were measured with a carbon resistor which had been calibrated against a CMN magnetic thermometer calibrated as described above.

D. Magnetic Phase Diagram

The phase diagram of $DyPO_4$ was obtained by locating the maximum in the heat capacity in a constant applied field for a number of different fields. In all cases, the field was applied along the c axis of the sample. The sample, a small single crystal of $DyPO_4$ in the shape of a parallelepiped, was varnished directly on to a carbon resistor, which served as a thermometer. A heater was then varnished to the sample and the entire assembly was suspended by fine cotton threads in a vacuum jacket. A weak thermal link to the bath consisted of a small copper wire, one end of which was varnished to the heater and the other end soldered to the shield which was in contact with the bath. The temperature at which the maximum of the heat capacity occurred could then be determined by monitoring the temperature as the sample was heated at a uniform rate in a constant magnetic field.

E. Optical Spectroscopy

The absorption spectrum of $DyPO_4$ was recorded on a 6.4-m photographic spectrograph with a Paschen mounting and a 1.8-m photoelectric spectrometer of the Fastie-Ebert design. The Paschen spectrograph was used for measurements of line position while the Fastie-Ebert spectrometer was used for line-intensity measurements. When accurate temperature measurement was necessary, the source light was passed through a monochromator and polarizer to reduce its total energy before it entered the crystal. A germanium resistance thermometer mounted 6 mm from the crystal was used to measure the temperature of the helium bath in which the crystal was directly immersed. The germanium thermometer was calibrated by the manufacturer against secondary standards traceable to the NBS provisional temperature scale No. 2-20 (1965).[23] Heating of the crystal by the excitation light was negligible.

IV. THEORY

Essam and Sykes[2] have considered the Ising model on a diamond lattice with nearest-neighbor exchange only. We shall summarize some of their results. The spin Hamiltonian for such a system with effective spin $S=\frac{1}{2}$ is

$$\mathcal{H}=\sum_{i>j}^{N}\frac{J}{S^2}S_{iz}S_{jz}+\sum_{i=1}^{N}g_{\parallel}\mu_B S_{iz}B_z \quad . \tag{1}$$

The pair summation is over the nearest neighbors only, J is the exchange parameter, and μ_B is the Bohr magneton. The critical parameters and other physical quantities were obtained by the method of series expansion. The critical temperature was estimated by finding the radius of convergence for the high-temperature expansion of the reduced susceptibility, $\xi=kT\chi/Nm^2$, where k is the Boltzmann constant, χ is the zero-field susceptibility, N is the number of spins, and m is the magnetic moment of each spin. The critical temperature estimated in this way is given by the expression

$$kT_N/qJ=0.6760, \tag{2}$$

where $q=4$ is the number of magnetic nearest neighbors in $DyPO_4$. The high-temperature expansion was made in terms of the parameter $v=\tanh(J/kT)$,

$$\xi=1+\sum_{n=1}^{\infty}a_n v^n \quad . \tag{3}$$

The first 16 coefficients were given by Essam and Sykes. In addition, they gave the high-temperature expansion of the logarithm of the partition function,

$$\ln\Lambda=\ln 2-2\ln(1+v)+\sum_{n=3}^{\infty}g_n v^{2n} \quad , \tag{4}$$

where terms through $n=8$ have been evaluated.

At temperatures below the transition temperature the energy and heat capacity were obtained as power series in $z=e^{-2J/kT}$:

$$\frac{E}{J}=U(z)=\sum_{n=2}^{\infty}e_n z^{2n} \quad , \tag{5}$$

$$\frac{C_v}{R}(\ln z)^2=\sum_{n=2}^{\infty}f_n z^{2n} \quad , \tag{6}$$

where $U(z)$ is the configurational energy and C_v is the heat capacity at constant volume. Essam and Sykes calculated the first 11 coefficients of

these series.

In another paper, Sykes, Essam, and Gaunt[26] have given an expression for the low-temperature reduced susceptibility of the same model considered by Essam and Sykes. That expression is

$$\xi = \sum_{n=2}^{\infty} b_n z^{2n} \quad , \tag{7}$$

where the first nine nonzero coefficients have been calculated.

Because the low-temperature series expansions for the diamond lattice converge up to the critical point, this model is well suited for studying critical behavior. Essam and Sykes concluded that the heat capacity must have a logarithmic singularity as T_N is approached from below. If the singularity is logarithmic above T_N also, they concluded that the amplitude below T_N is about 2.5 times larger than the amplitude above T_N. They stated, however, that logarithmic divergences below and above the critical point are mutually exclusive and that the divergence above T_N is probably not logarithmic. They did not, however, appear to consider their analysis as conclusive. Gaunt and Domb,[27] on the other hand, assume that the heat capacity in the critical region has the asymptotic form

$$\frac{C}{R} = \frac{A^{\pm}}{\alpha} t^{-\alpha} - B^{\pm} \quad , \tag{8}$$

where $t \equiv |T - T_N|/T_N$ and $\alpha = \frac{1}{8}$. Starting from this assumption, they obtained a more detailed representation which becomes the series derived by Essam and Sykes for low temperatures, i.e., for $t > 10^{-1}$. They concluded that the critical region exists only for $t \lesssim 10^{-4}$ and that in the region 4×10^{-4} to 4×10^{-2} their results *appear* to be logarithmic.

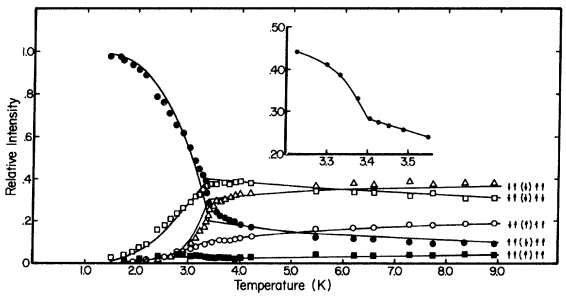

FIG. 2. Relative intensities of each of the five lines in $DyPO_4$ as function of temperature. The points are the experimental relative intensities and the solid lines are the results of a theoretical BPW calculation. Each line has been labeled on the right by the nearest-neighbor spin configuration associated with it. The insert is an enlarged portion of the critical region. A solid line has been drawn through the experimental points in the insert. All measurements were made for the Z_1-L_2 transition of $DyPO_4$ in the π polarization.

TABLE I. Quintet spacings and derived exchange parameters for five optical transitions observed in $DyPO_4$.

Level observed	Quintet spacing in π polarization (cm^{-1})	Spacing in σ polarization (cm^{-1})	$\frac{J}{hc}$ (cm^{-1})	$\frac{J'}{hc}$ (cm^{-1})
F_1	2.41±0.1	1.26±0.1	0.92±0.05	0.29±0.05
J_2	unresolved	1.49±0.07	...	0.17±0.09
L_2	2.93±0.1	0.75±0.1	0.92±0.05	0.54±0.05
M_1	...	1.82±0.1	...	0.01±0.1
M_2	...	1.71±0.1	...	0.06±0.1

The theoretical results derived by Essam and Sykes,[2] Sykes, Essam, and Gaunt,[26] and Gaunt and Domb[27] will be compared with the magnetic-susceptibility and heat-capacity results. Since the necessary pair-correlation function has not been calculated, the optical results have not been included in this comparison.

V. RESULTS AND DISCUSSION

A. Optical

The spectrum of $DyPO_4$ is characterized by small groups of five equally spaced lines that appear in place of the single lines of dilute $Dy:YPO_4$. Except for these groups, the general spectral features of the two materials are identical, suggesting that the groups have a magnetic origin. Although the total intensity within any of these groups remains the same, the relative intensities of the five lines within the group change as a function of temperature. The relative intensities were measured photoelectrically for a variety of temperatures. The measurements were accurate to 6% for temperatures above 2.4 K, but below this point overabsorption of the lines limited the accuracy to 10%. The results are shown in Fig. 2 together with a theoretical calculation, shown as smooth curves, of the intensities that will be discussed later. It is important to note the sudden change in the relative intensities that occurs at 3.40 K and the disappearance of all but one line at low temperatures.

The spacings between the lines of the five-line groups are given in Table I for five transitions that have well-resolved lines. The transitions that are allowed in both the σ and π polarizations have different line spacings for each polarization.

The linewidths within the substructure exhibit the temperature dependence shown in Fig. 3. The linewidths within a given quintet are all the same within the experimental error (± 10%) but vary greatly between different quintets, depending on the single-ion transition observed. There are many lines whose breadth totally obscures the five-line structure. Such lines are usually the upper members of a Stark group, and, therefore, their breadth is probably due to single-phonon relaxation.[28] The widths of the resolved five-line pattern seem to

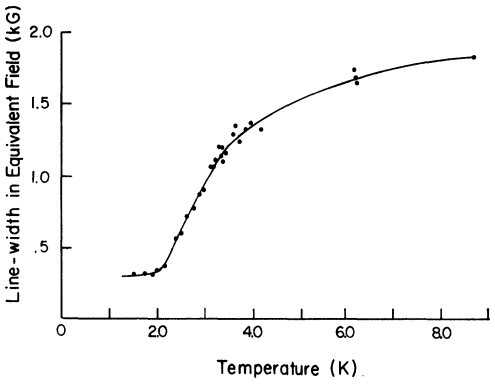

FIG. 3. Half-width at half-maximum of a single line in the five-line pattern of $DyPO_4$ as a function of temperature. The half-width has been expressed as an effective magnetic field which acts upon both the ground and excited states.

depend upon the splitting factor of the state observed. When the linewidth is expressed in terms of an effective magnetic field acting on both the excited and ground states, the results are, therefore, roughly independent of the single-ion transition observed. Thus, the linewidths in Fig. 3 have been expressed in terms of an effective magnetic field.

The highest energy line of the five-line pattern associated with the Z_1-L_2 transition appeared to exhibit a very small (0.2 ± 0.2 cm^{-1}) shift in position to lower energy as the temperature was lowered from 4.2 to 1.5 K. This shift corresponds to a (0.27 ± 0.27)-kG effective field which acts on both the ground and excited states. The adjacant line appears to shift to lower energy also, while the two lowest energy lines of the five-line pattern appear to shift to higher energy.

The spectrum changes quite dramatically when an external magnetic field is applied along the c axis of the crystal. The behavior of the five-line pattern associated with the Z_1-L_2 π-polarized transition is shown in Fig. 4 for a temperature of 1.5 K. At this temperature, only the two highest energy lines and the lowest energy line can be observed in zero field, the highest energy line being the most intense. When the external field is applied, this line splits linearly into two lines of equal intensity up to about 4.5 kG. Then the slopes increase sharply (see Fig. 4) and the higher energy line rapidly disappears. The widths of the lines increase by a factor of 1.7 over those at lower fields. Also, the other lines of the quintet appear in this region. The line that originated at the low-energy side of the quintet now becomes the predominant line. At ~10 kG, only one line remains and its slope is again linear. If the high-field line is extrapolated back to lower fields, there is a (4.8 ± 0.5)-kG discontinuity between the two regions (see Fig. 4). The lines in the σ polarization have exactly the same behavior as that discussed above. Since the lines in the σ and π polarizations at high field correspond to transitions from the ground state to each member of the Kramers excited state, a value of $g_{\parallel}$ can be extracted for the ground and excited states from the high-field slopes of the two polarizations. We do not expect that this measurement is affected by changes in the internal magnetization since the linearity of the slopes from 10 to 36 kG indicates that the magnetization has already reached saturation. We find $g_{\parallel} = 19.5 \pm 0.4$ for the ground state of $DyPO_4$.

The spectrum changes only slightly when a magnetic field is applied perpendicularly to the optic axis. A value of 0.5 ± 0.5 has been determined for $g_{\perp}$ of the ground state. The large inaccuracy is due to uncertainties in orienting the crystal. There are no intensity changes of any of the lines for a field applied perpendicularly to the c axis.

The measured value of $g_{\parallel}$ is quite striking. The ground term of Dy^{3+} is a $^6H_{15/2}$ state which would have a Landé factor of $\frac{4}{3}$. Using intermediate coupling calculations, Wybourne[29] refines this value to 1.312. A pure $J_z = \pm\frac{15}{2}$ ground state would produce the largest possible splitting in a parallel field,

$$g_{\parallel} = 2\Lambda J_z = 19.680 \quad ,$$

but would have no splitting in a perpendicular field,

$$g_{\perp} = 0.$$

Comparing these values with those observed,

$$g_{\parallel} = 19.5 \pm 0.4, \quad g_{\perp} = 0.5 \pm 0.5 \quad ,$$

the ground state must be an almost pure $J_z = \pm\frac{15}{2}$

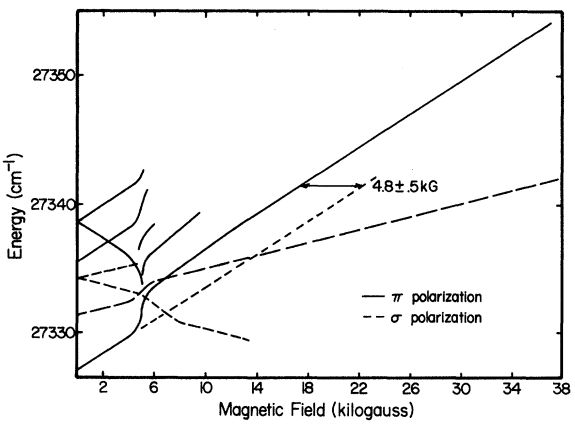

FIG. 4. Parallel Zeeman splitting of the $DyPO_4$ Z_1-L_2 transition at 1.5 K. Note that when the energy of the *observed* line is increasing, the energy of the ground state is decreasing because the ground-state splitting is larger than the excited-state splitting.

state. Since Levy[30] has shown that interionic interactions are capable only of coupling states differing in J_z by 7, there can be no off-diagonal operators coupling $+\frac{15}{2}$ to $-\frac{15}{2}$. The only possible interactions must be diagonal, and thus can be expressed as the Ising interaction Eq. (1). If there are small admixtures of a lower value of J_z present, these could lead to off-diagonal operators but one would expect such effects to be very small. The five-line substructure of the absorption lines then results from the splitting of the Kramers degeneracy of a single ion by interactions with four neighboring Dy^{3+} ions. If all four neighboring Dy^{3+} ions have moments pointing in the same direction along the c axis, the Kramers degeneracy of a single ion will be split by $8J$. If one of the neighbors has a moment directed opposite to the other three, the splitting is $4J$. If two neighboring moments are oppositely directed from the other two, there will be no splitting. Thus, there will be three different spin arrangements in the crystal which depend only upon the magnetic-moment arrangement of the four neighboring ions about a central ion. The population of each of these three spin arrangements will be temperature dependent. In particular, the arrangement with the four neighbors aligned will predominate (they are all on the same sublattice) when the crystal orders antiferromagnetically. There will also be interactions between the ground states of the four neighbors and the excited states of the central ion. If this interaction is also Ising-like, i.e.,

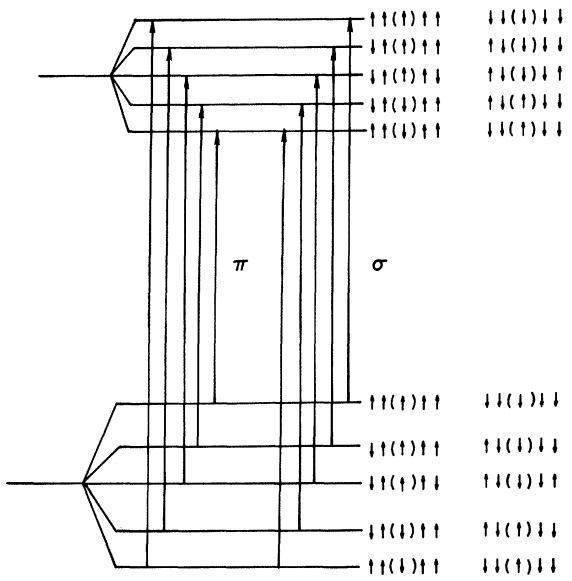

FIG. 5. Zero-field splittings of the ground and excited states and the allowed transitions between them. The splittings correspond to the different spin arrangements of an ion with its nearest neighbors.

TABLE II. Dipolar fields at a given ion on sublattice 1 calculated for several neighbor shells.

Neighbor shell no.	Spins per shell	Field per spin (G)	Sublattice for shell
1	4	828	2
2	4	−438	2
3	8	−81	1
4	2	817	1
5	4	−274	1
6	8	165	2
7	4	−233	2
8	8	29	2
9	8	35	1
10	4	−97	1

$$\mathcal{H}=\sum_{i=nn}\frac{J'}{S^2}S_{0z}S_{iz}\quad,$$

the Kramers degeneracy of the excited state will be split by $8J'$, $4J'$, and 0, respectively, for the three different spin arrangements. The optical transitions observed occur between ground and excited states where the type of arrangement has not changed (none of the four neighbors changes its moment direction) and for which appropriate selection rules are obeyed. The transitions from a given Kramers ground state to either of the two split Kramers excited states occur in different polarizations, either the σ or π polarization. The result is a series of five equally spaced lines in each polarization with different spacings for the two polarizations. Figure 5 indicates these allowed transitions. The four outer arrows refer to the magnetic-moment direction of the four neighboring ions and the arrow in the parenthesis refers to the direction of the central ion. The value of the exchange constant for both the ground and the excited states of Dy^{3+} can be obtained by measuring the spacings of the quintet patterns in both polarizations. The values are given in Table I.

Since the magnetic moment of the ground state is known, the dipolar contribution to J of different shells of neighbors could be computed; it is summarized in Table II. It is evident that dipolar contributions are not sufficient to explain the entire splitting, although the nearest-neighbor contribution can explain almost half the total splitting. The question now arises as to which quartet of neighbors actually produces the observed five-line pattern. It seems likely from examining Table II and the crystal structure that the interaction with the four nearest neighbors (nn) is the predominant interaction and is the cause of the observed five-line pattern.

The orientation of the moments corresponding to the lines of the quintet may be deduced from the parallel Zeeman effect. The line that persists at high fields must correspond to the configuration

where all the moments are aligned. This line originates from the lowest energy line of the quintet, as can be seen in Fig. 4. The highest energy line then must correspond to the configuration where all the nn are aligned and the central ion is oppositely directed. Since this is the only line that persists at low temperatures, all the ions in the crystal must have this configuration of nn and the crystal must, therefore, be ordered antiferromagnetically. The arrows in Fig. 1 illustrate this type of order.

Since each line of a five-line pattern corresponds to a definite magnet-moment arrangement of a central ion and its four neighbors, the relative numbers of various near-neighbor moment configurations can be determined by measuring relative intensities. When the crystal orders antiferromagnetically, the intensity of the line corresponding to antiferromagnetic alignment of a given ion and its four neighbors increases suddenly. The sudden increase is shown in Fig. 2 in the enlarged insert. This behavior has been used to determine a Néel temperature for $DyPO_4$ of 3.40 ± 0.04 K, in good agreement with the heat-capacity and susceptibility measurements.

The relative intensities of the five lines as a function of temperature have been fitted using a Bethe-Peierls-Weiss (BPW) approximation to an Ising model. This approximation treats a cluster of an ion and its nearest neighbors exactly and approximates the rest of the lattice as an internal field which acts only on the nearest neighbors.[31] The short-range order within the cluster can thus be taken into account exactly, but short-range order of any extent greater than the immediate cluster is not treated. The magnitude of the internal field is determined by the self-consistence condition that the average value of the spin of a given ion is the negative of the average value of the spin on a nearest-neighbor ion (since the material is antiferromagnetic). The Hamiltonian

$$\mathcal{H} = \sum_{i=1}^{4} \sum_{s_z = \pm 1/2} \left(\frac{J}{S^2} S_{0z} S_{iz} + g_{\parallel} \mu_B S_{iz} H_I \right) \tag{9}$$

is used, where S_{0z} represents the spin of the central ion, S_{iz} is the spin of the nearest neighbors, and H_I is the internal field acting only on the near neighbors. The partition function is then

$$Z = \sum_n g_n e^{-E_n/kT} \quad , \tag{10}$$

where E_n is an eigenvalue of the Hamiltonian, g_n is the degeneracy of each eigenvalue, and the sum is over all eigenvalues. Each eigenvalue corresponds to a level of the ground-state quintet. The relative intensities of the lines originating from this ground-state quintet can then be easily obtained from the partition function[32]:

$$I_m = \binom{m}{4} \exp[(4-2m)J/kT] \times \{\exp[(4-2m)\, g_{\parallel} \mu_B H_I / 2kT] + \exp[-(4-2m) g_{\parallel} \mu_B H_I / 2kT]\}/Z \, , \tag{11}$$

where m now represents the number of nearest neighbors antiferromagnetically aligned with the central ion, and

$$\binom{m}{4}$$

is a binomial coefficient. The value of J used in Eq. (11) is not the one determined from the quintet spacings, but rather has been calculated from the observed Néel temperature. For the BPW approximation, the relation between the Néel temperature and J is

$$\frac{kT_N}{J} = \frac{1}{2 \ln[q/(q-2)]} = 0.7213 \quad , \tag{12}$$

where q is the number of nearest neighbors.[31] If the value of J obtained from the quintet spacings were used, we would obtain a Néel temperature 0.4 K higher than that actually observed. Molecular field approximations are expected to predict higher-ordering temperatures, however.

The results of the theoretical approximation are shown in Fig. 2 along with the measured values. Note that the measured antiferromagnetic line intensity near the transition temperature is higher than that calculated. The BPW model has been restricted to treat exactly only the nn cluster, but since the short-range order extends further than the nn when approaching the Néel temperature, we would expect that the number of ions with an antiferromagnetic configuration would be underestimated by the approximation. At higher temperatures, the relative intensities of the lines approach the statistical weights of 1:4:6:4:1 that would be expected for a system without interactions.

An indication of the importance of coupling with other neighbors can be obtained from the linewidths of the observed lines. There will be a temperature-dependent and a temperature-independent contribution to the linewidths. The intrinsic linewidth is caused by perturbations of the crystal field and by lifetime broadening. The temperature-dependent width is caused by interactions with neighbors other than nn; since these interactions with other shells of neighbors can be treated as a perturbation of the nn interaction, they give rise to unresolved multiplet patterns within each line of the quintet, in the same way as the quintet pattern itself is formed. Because of the finite breadth of their lines and the large number of ions, the result is a broad line. The contribution of the dipolar interaction to this

width from the further shells of neighbors has already been presented in Table II. It can be seen that the dipole interactions give the right order of magnitude for the half-widths of the lines observed in Fig. 3. The relative intensities of the unresolved multiplet lines will also have temperature dependences similar to that of the nearest neighbors, and it is expected that these lines would narrow as the temperature is lowered. If there is a net interaction with other neighbors, the center of the line would also shift with temperature.

Although the linewidths indicate that there are significant interactions with more distant neighbors, the sum of all these interactions is very small in the antiferromagnetic state. This can be seen from the very small (0.27 ± 0.27 kG) shift in the positions of the five lines between 4.2 and 1.5 K. Since the sublattice magnetization is almost saturated at 1.5 K, such a shift corresponds to the total additional interactions present in the ordered state. The shift of the two high energy lines toward the red indicates that the additional field is directed oppositely to the ordered moments. We expect the two lowest energy lines to shift toward the blue, as observed, because the most probable configuration for these lines is for the nearest neighbors to be close to perfect alignment, but for the central ion to be flipped from the perfectly aligned configuration. The internal field acting on the central ion is then in the opposite direction. Thus, this small temperature-dependent shift in line position is an indication that there is only a small *net* interaction with neighbors further than the nearest neighbors.

To determine the dipolar contribution to this small shift in line position, a dipolar sum was performed over all the ions within a sphere of radius 90 Å. The dipolar sum was performed over each sublattice separately. The sum over all the ions on the same sublattice as the ion at the center of the sphere is defined as H_{1d}. Since the nearest neighbors do not contribute to any shift in line position, the sum over the opposite sublattice (H_{2d}) does not include the nearest neighbors. The results of the sum are

$$H_{1d} = 0.112 \text{ kOe}, \quad H_{2d} = -1.230 \text{ kOe} \quad ,$$

where a positive sign indicates a field directed along the ordered moment when the lattice is ordered antiferromagnetically. The total field acting on an ion in the antiferromagnetic state must also include any exchange fields from the two sublattices,

$$H_T = (H_{1d} + H_{2d}) + (H_{1e} + H_{2e}) \quad . \tag{13}$$

Since we observe $H_T = -0.270$ kG, then

$$(H_{1e} + H_{2e}) = 0.848 \text{ kG} \quad . \tag{14}$$

Additional exchange interactions which cancel most of the dipolar contributions must, therefore, be present.

The behavior of the $DyPO_4$ spectrum in the 4–6-kG region of the parallel Zeeman effect (see Fig. 4) is associated with the metamagnetic phase transition. At low fields and low temperatures the two-sublattice antiferromagnetic arrangement is not affected by the external field. Since the external field lies along the moments of one sublattice, but is opposed to the moments of the other sublattice, the degeneracy of the two sublattices is removed by the field. The line corresponding to the antiferromagnetic configuration splits linearly, therefore, into two lines of equal intensity. Such a splitting is commonly called a pseudosplitting because it arises from energy changes in two different ions rather than from splittings of single-ion levels. Near the transition field many spins flip in the direction of the field. There is a corresponding decrease in the number of arrangements having the central ion aligned with a field and its four neighbors aligned opposite to the field (corresponding to the highest energy line), a smaller decrease in the number having the four neighbors aligned with the field and the central ion aligned opposite (corresponding to the lower energy of the pseudosplit lines), and an increase in the number with the central ion and its four neighbors all aligned with the field (corresponding to the lowest energy line).

The critical field and temperature for the metamagnetic transition can be determined in exactly the same manner as the Néel temperature, by finding the point at which the intensity of the antiferromagnetic line suddenly decreases. This critical point has been determined for a number of temperatures and fields in order to obtain the phase diagram for $DyPO_4$ shown in Fig. 6. The only point on the

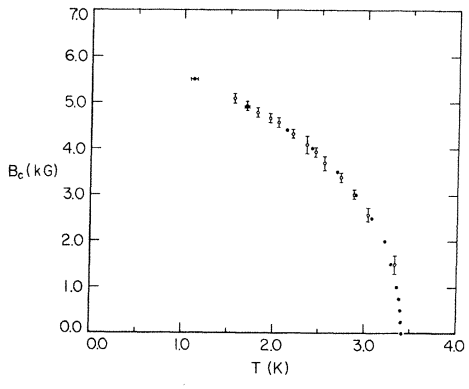

FIG. 6. Magnetic phase diagram of $DyPO_4$ at temperatures above 1 K. The solid circles represent the data obtained by locating the maximum in the heat capacity in a given field B. The open circles represent the data obtained from the spectroscopic measurements. The vertical and horizontal lines represent the estimated error in the measurements.

phase diagram that can be determined theoretically is the critical field at 0 K. The metamagnetic transition will occur when the free energy of the ferromagnetic state (a saturated paramagnetic state) is equal to the free energy of the antiferromagnetic state.

The free energy of a crystal of N ions at 0 K in the ferromagnetic state is

$$F_f = \tfrac{1}{2}N\mu\,[qJ/\mu - \tfrac{1}{3}4\pi M_0 - (H_{1d}+H_{1e}) + (H_{2d}+H_{2e}) - 2H_0] \quad , \tag{15}$$

where M_0 is the saturation magnetization, and a factor of $\frac{1}{2}$ has been introduced to avoid counting moments twice. The demagnetizing field has been omitted because it leads to a mixed phase state.[33] The free energy of the crystal in the initial antiferromagnetic state is

$$F_{af} = \tfrac{1}{2}N\mu\,[qJ/\mu + (H_{1d}+H_{1e}) + (H_{2d}+H_{2e})] \quad . \tag{16}$$

The critical field at 0 K is, therefore,

$$H_c = qJ/\mu - \tfrac{1}{2}[\tfrac{4}{3}\pi M_0 - 2(H_{2d}+H_{2e})] \quad . \tag{17}$$

In order to evaluate this expression, we must first determine H_{2e}.

As the system passes through the critical region into the ferromagnetic phase, there is a change in the slopes of the lines due to the additional internal fields present in the new phase. This change in slope is clearly shown in Fig. 4, where the additional fields result in a (4.8 ± 0.5)-kG discontinuity in the line splittings. There are several fields that contribute to this discontinuity. In the ferromagnetic state the contributions are from the Lorentz and demagnetizing fields. If the spectral line corresponding to ferromagnetic alignment is followed (see Fig. 4), there is also a contribution from the sum of all ions on the same sublattice as the central ion, since all of these ions reverse their spins. The ions on the opposite sublattice have not changed. The size of the discontinuity is, therefore,

$$H_{\text{discont}} = \tfrac{4}{3}\pi M_0 - DM_0 + 2(H_{1d}+H_{1e}) \quad , \tag{18}$$

where DM_0 is the demagnetizing field which must now be considered. Since the saturation magnetization can be calculated from both the magnetic moment and the density of ions, and since the demagnetizing factor D can be estimated, this equation

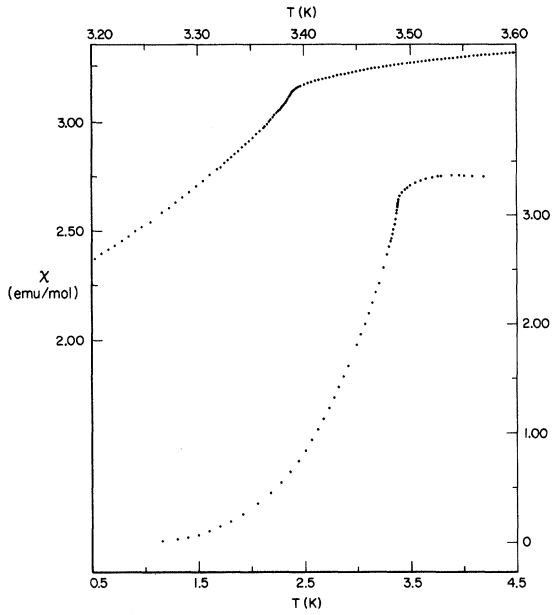

FIG. 7. Magnetic susceptibility of $DyPO_4$ as a function of temperature. The solid circles are the data points for a single crystal with the shape of a parallelepiped ($D \sim 0.9$). The ordinate and abscissa for the lower curve are those on the right-hand side and bottom of the figure, respectively. The ordinate and abscissa for the upper curve are those on the left-hand side and top of the figure, respectively. Note that the temperature scale at the top has been expanded by a factor of 10 from that at the bottom of the figure.

can be solved for H_{1e}. Equation (14) may then be used to find a value of H_{2e}. The values for H_{1e} and H_{2e} have been summarized in Table III. The critical field at 0 K can now be found from these data. Using the measured values of J and H_{2e}, we find that

$$H_c(T=0\text{ K}) = 5.20 \pm 0.52\text{ kG} \quad .$$

This predicted value of the critical field can be compared with the experimental values given in Fig. 6. Since no data are available below 1.5 K at this time, extrapolation of the phase diagram to 0 K cannot be done accurately. It is evident from Fig. 6, however, that the critical field at 0 K is close to that predicted.

All of the important results obtained for $DyPO_4$

TABLE III. Important parameters of $DyPO_4$.

Calculated values		Measured values		Predicted values	
H_{1d}	0.112 (kOe)	qJ/μ	8.073 ± 0.44 kOe	H_{1e}	-0.12 ± 0.25 (kOe)
H_{2d}	-1.23 (kOe)	μ	0.455 ± 0.009 cm^{-1}/kG	H_{2e}	0.97 ± 0.52 (kOe)
M_0	1.249 (kOe)	H_{discont}	4.8 ± 0.4 kG	$H_c(T=0\text{ K})$	5.20 ± 0.52 (kG)
DM_0	0.408 (kOe)	H_{shift}	-0.27 ± 0.27 kG		
$\frac{1}{3}4\pi M_0$	5.231 (kOe)				

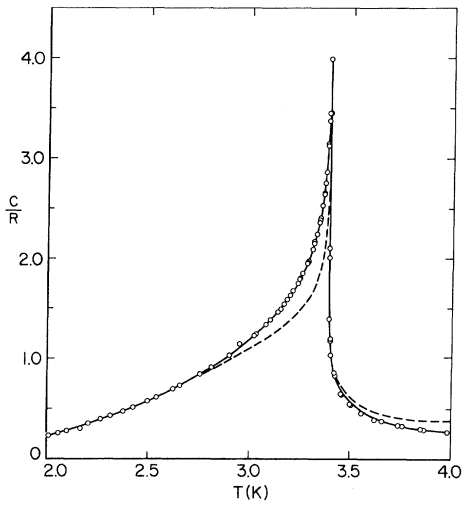

FIG. 8. Magnetic heat capacity of $DyPO_4$ in the transition region. The open circles are the data points. The solid line is the theoretical curve as described in the text. The dashed line is the curve of $d(\chi T)/dT$ (normalized at 2 K) calculated from the magnetic susceptibility which has been corrected to the shape appropriate for comparison with the heat capacity and the series expansions (Refs. 36 and 38).

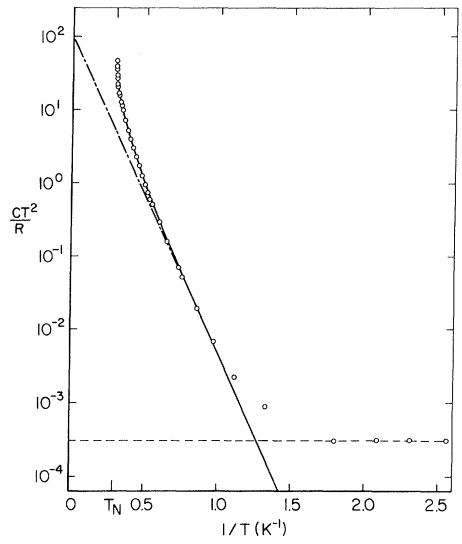

FIG. 9. $\log_{10}(CT^3/R)$ as a function of $1/T$. The open circles are the data points. The solid line is the theoretical curve of Essam and Sykes. The dot-dashed line is the low-temperature limiting curve one would obtain in the absence of hyperfine interactions. Its slope and intercept are uniquely determined in the low-temperature limit. The dashed line indicates the hyperfine contribution to the heat capacity.

have been summarized in Table III. The measured values given in this table were obtained directly from experimental observations. The calculated values were based upon the measured magnetic moment and the published crystal structure. Both the measured and calculated values were used to obtain the predicted values in the table.

B. Magnetic Susceptibility and Heat Capacity

The parallel magnetic susceptibility of $DyPO_4$ was measured in both the liquid-hydrogen and liquid-helium temperature ranges, while the heat capacity was measured in the liquid-helium range.

The low-temperature magnetic-susceptibility results for a single crystal in the shape of a parallelepiped ($D \sim 0.9$) are shown in Fig. 7. After passing through a gentle maximum at about 4.00 K the susceptibility falls off sharply below 3.5 K. The point of maximum slope is at the transition temperature, which is 3.388 ± 0.005 K. The heat-capacity results are shown in Fig. 8. The Néel temperature, determined as the maximum in the heat-capacity curve, is 3.390 ± 0.002 K.

The only adjustable parameter in the series expansions is the nearest-neighbor exchange interaction J. Not only can this parameter be determined from the optical splitting, but it can also be estimated from the low-temperature asymptotic forms of the heat capacity and the reduced susceptibility. For an Ising system described by the Hamiltonian, Eq. (1), these quantities have the following forms in the low-temperature limit:

$$C/R = (2qJ/kT)^2 e^{-2qJ/kT} \quad , \quad \xi = A\, e^{-2qJ/kT} \quad . \tag{19}$$

When $\log_{10}(CT^2/R)$ is plotted vs $1/T$, a given

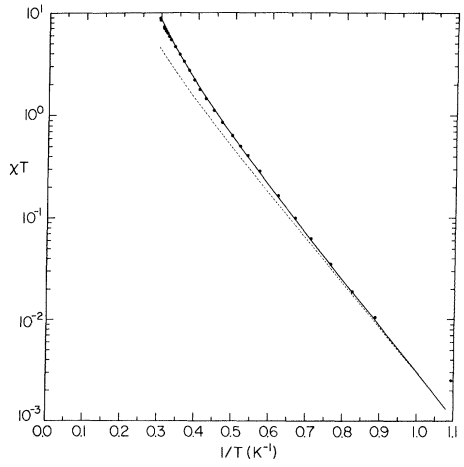

FIG. 10. $\log_{10}\chi T$ as a function of $1/T$. The solid circles represent the experimental data corrected to the shape appropriate for comparison with theory (Refs. 26 and 36). The solid line is the theoretical curve calculated from the low-temperature series expansion for the energy. The dashed line is that calculated from the low-temperature series expansion for χT.

value of J uniquely determines both the slope and the intercept, as shown in Fig. 9. Whereas, when $\log_{10}\xi$ is plotted against $1/T$ as shown in Fig. 10, the slope alone determines J. The experimental values so obtained are shown in Table IV. It is also possible to use Eq. (2) to determine a value of J from the measured value of T_N. As shown in Table IV, the value of J determined from T_N is in good agreement with the values determined by the other methods. Since the precision of measurement of T_N is much better than that for the other measurements, the value of J determined from T_N will be the one used in the comparison of theory with experiment. Essam and Sykes have calculated values for E_c/J and S_c/k. The experimental values of the critical energy and entropy can be obtained by integrating the heat-capacity data, and the results, shown in Table V, are in good agreement with the theoretical estimates

Using the value $J/k = 1.25$ K, the theory of Essam and Sykes can be compared with the experimentally determined magnetic susceptibility and heat capacity. In Figs. 8 and 9, the low-temperature expansion for the heat capacity, Eq. (6), is plotted as solid lines, and the open circles represent the data. There is excellent agreement except at very low temperatures, where the hyperfine interaction (indicated by the dashed line in Fig. 9) dominates. Cooke and Park[34] have noted that the ratio of the nuclear hyperfine constant to the spectroscopic splitting factor should be independent of the particular state of the Dy^{3+} ion. From EPR measurements of Dy^{3+} in $Dy(CH_3COO)_3 \cdot 4H_2O$, they find for ^{161}Dy, $A/g_{\parallel} = 0.00280$ cm^{-1} and for ^{163}Dy, $A/g_{\parallel} = 0.00397$ cm^{-1}. Park[35] has measured the EPR of Dy^{3+} in the double nitrate and shown that for ^{161}Dy, $A/g_{\parallel} = 0.002713$ cm^{-1} and for ^{163}Dy, $A/g_{\parallel} = 0.003783$ cm^{-1}. Also, for ^{163}Dy, $B/g_{\perp} = 0.003833$ cm^{-1} and for ^{161}Dy, $B/g_{\perp} = 0.00276$ cm^{-1}. In $DyPO_4$, $g_{\parallel} = 19.5$ and the natural abundances of ^{161}Dy and ^{163}Dy are 18.7 and 25%, respectively; thus, using the values of Cooke and Park in the relation

$$CT^2/R = \tfrac{1}{9}A^2[S(S+1)][I(I+1)]$$

for each isotope, we find that the hyperfine contribution to the heat capacity should be about $CT^2/R = 0.00308$, whereas our measured value is 0.00033 ± 0.00003, or nearly an order of magnitude smaller.

TABLE IV. Comparison of exchange parameters determined by different methods.

Method of determining J	Value of J/k
Asymptotic heat capacity	1.25 ±0.02
Asymptotic susceptibility	1.25 ±0.02
Quintet splitting	1.32 ±0.07
Calculated using kT_N/qJ and T_N from heat-capacity maximum	1.254±0.001

TABLE V. Comparison of experimental and theoretical values of the entropy and energy at the critical point.

	Experimental	Theoretical
S_c/k	0.505	0.5113
E_c/kT_N	0.408	0.418

This indicates that the hyperfine interaction in $DyPO_4$, as determined from the heat capacity, is about $\frac{1}{3}$ of that in $Dy(CH_3COO)_3 \cdot 4H_2O$. It is possible that thermal contact was lost with a large portion of our sample at these lower temperatures, resulting in low values of the heat capacity. There was, however, no indication from the behavior of the system during the measurements that this was occurring.

The low-temperature expansion for the susceptibility derived by Sykes, Essam, and Gaunt is indicated by the dotted line in Fig. 10 and the solid line in Fig. 11. The magnetic susceptibilities in both figures have been corrected to the shape appropriate for comparison with the series expansions.[26,36] This disagreement with the experimental results is most surprising in view of the agreement of the theory with the heat-capacity data. To investigate this further, we make use of the relation

$$C \simeq A \frac{\partial(\chi T)}{\partial T} , \qquad (20)$$

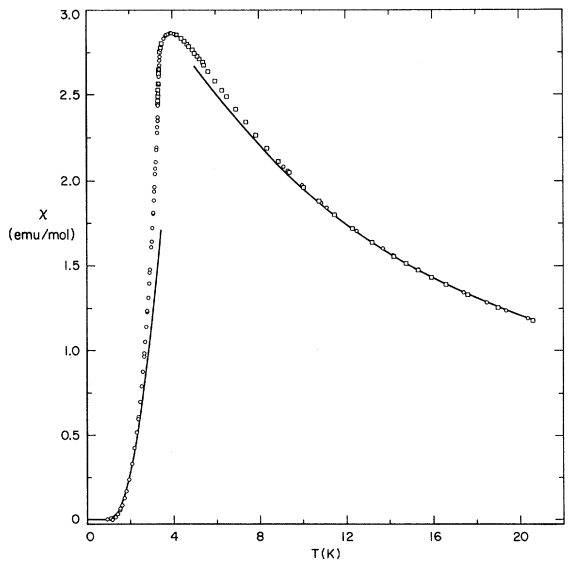

FIG. 11. Plot of the magnetic susceptibility as a function of temperature. The open circles and squares represent the data obtained in different runs on the same crystal and which have been corrected to the shape appropriate for comparison with the series expansions (Refs. 26 and 36). The solid lines were calculated from the low- and high-temperature series expansions for χT.

given by Fisher[37] relating the susceptibility and the heat capacity of an antiferromagnet. In the above expression, A is believed to be a slowly varying function of T.[38,39] A comparison of $\partial(\chi T)/\partial T$, calculated from the measured susceptibility, with the measured heat capacity is shown in Fig. 8. Since the dipolar effects in $DyPO_4$ are large, the susceptibility has been corrected to the shape appropriate for comparison with the heat capacity and the series expansions.[26,36,38] The agreement at low temperatures is excellent, but that near the critical point and above is not as good. This is not surprising since we assumed that the function A is independent of temperature, which it almost certainly is not. The correspondence between the two peaks confirms, however, that it is the maximum in $\partial(\chi T)/\partial T$, rather than that in χ, which indicates the onset of long-range order, as has similarly been shown for other materials.[38–40]

The integrated form of the function given in Eq. (20) indicates that the configurational energy should be roughly proportional to the reduced susceptibility, where the proportionality constant should again be a slowly varying function of temperature. If the exact low-temperature expansion for the energy, Eq. (5), is plotted vs $1/T$, we indeed find excellent agreement with the data as indicated by the solid line in Fig. 10. This suggests that the variation of A with temperature could be found by plotting the reduced susceptibility as a function of the energy obtained by integration of the experimentally measured heat capacity. As shown in Fig. 12, the proportionality constant between the energy and the reduced susceptibility does indeed vary slowly with temperature. Since the susceptibility and heat-capacity results seem quite consistent with each other and with the low-temperature expansion for the energy, it is rather surprising that the expansion of Sykes, Essam, and Gaunt fails to give good agreement with experiment. The reason for this discrepancy is not known.

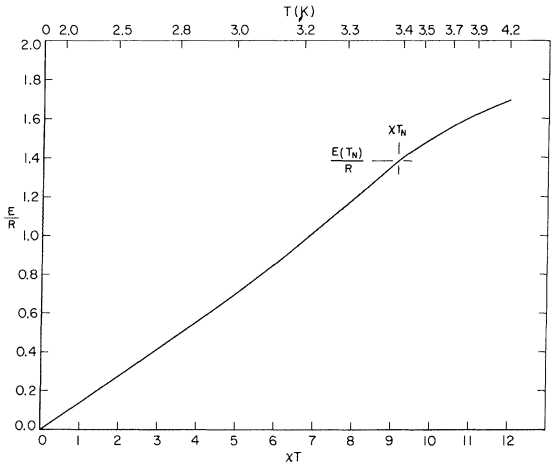

FIG. 12. Plot of E/R as a function of χT. The temperature is shown by the scale at the top of the figure. The values of the energy and χT at T_N are indicated. The solid line is a smooth curve through the various experimental values of E/R and χT determined at given values of T.

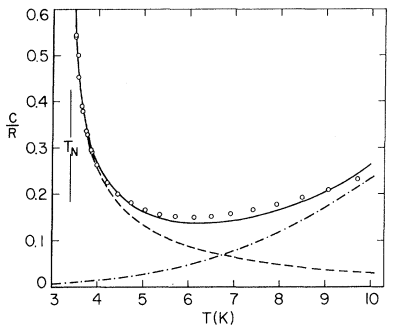

FIG. 13. High-temperature heat capacity of $DyPO_4$. The open circles are the experimental points. The dashed curve is the exact series expansion. The dot-dashed curve is the lattice contribution derived for $\theta_D = 100$ K. The solid curve is the sum of the two dashed curves.

The results for the susceptibility in the liquid-hydrogen region are shown in Fig. 11. The data have been corrected to the shape[36] appropriate for comparison with the theory.[26] Upon inserting the value $J/k = 1.25$ K into the high-temperature series expansion for the susceptibility as derived by Essam and Sykes, one calculates the solid curve shown in Fig. 11. As can be seen, experiment and theory are in good agreement.

The heat-capacity data extending to temperatures well above T_N are shown in Fig. 13. The dashed curve represents the expected contribution of the magnetic phase transition [Eq. (32)] to the total heat capacity. The dot-dashed curve represents a T^3 contribution to the heat capacity which was chosen to account best for the remaining heat capacity. This remainder is used to account for the lattice heat capacity of the sample, as well as addenda contributions which were not determined separately (see above). The sum of the two dashed curves is shown as the solid curve in the figure. The agreement of the calculated curve with the data is fairly good, but the discrepancy is large enough to make one look for other explanations. The first excited Kramers doublet is located 70 cm^{-1} above the ground state[41] and would have little effect on the heat capacity in this region. One cannot rule out a contribution from the phase transition which is not accounted for by the high-temperature series expansion. Using the series expansions to extrapolate the data to high and low temperatures, the total entropy change calculated from the experimental

heat capacity is $\Delta S/R = 0.69 \pm 0.01$. This is in close agreement with the theoretical value of $\Delta S/R = \ln 2 = 0.693$. An excess heat capacity as occurs between the data and the calculated curve in Fig. 13 would only increase the total entropy change by $\sim 0.007R$ or $\sim 1\%$, which is within the experimental uncertainty. One cannot, therefore, be certain that the theoretical expression gives an accurate representation of the magnetic heat capacity above 4 K.

In practice, the exact series expansions are truncated infinite series which can accurately represent the physical quantities only in the regions away from the critical point. In the present case, both the high- and low-temperature series become inaccurate within about 10% of T_N. Usually the coefficients in the series settle down to a regular pattern of behavior after the first few terms so that it is possible to find an expression which approximates the actual coefficients and can be used to evaluate terms beyond those determined by statistical methods. In their evaluation of the low-temperature series, Essam and Sykes found that the coefficients e_n in the energy expansion Eq. (5) could be represented at large n by

$$e_n = 0.825\,[(n-1)(n-2)z_c^{2n}]^{-1} \quad , \tag{21}$$

and the energy could then be written as

$$\frac{E}{J} = \sum_{n=2}^{12} e_n z^{2n} + \sum_{n=13}^{\infty} \frac{0.825}{(n-1)(n-2)} \left(\frac{z}{z_c}\right)^{2n} \quad . \tag{22}$$

This expression can be rewritten in a form which is easily evaluated at all temperatures,

$$\frac{E}{J} = \sum_{n=2}^{12} e_n z^{2n} - \sum_{n=3}^{12} \frac{0.825}{(n-1)(n-2)} w^n + 0.825\,[w(1-w)\ln(1-w) + w^2] \quad , \tag{23}$$

where $w = (z/z_c)^2$.

In Fig. 14 the solid curve for $T < T_N$ is the temperature derivative of Eq. (23). The agreement between theory and experiment is remarkable, having a maximum deviation of only 2% over the range 1 K to within 0.1% of T_N. It is the last term in Eq. (23) that determines the limiting logarithmic behavior of the heat capacity as T approaches T_N. It becomes

$$C/R = -0.45 \ln t + 0.56 \quad . \tag{24}$$

The high-temperature expansion can be extrapolated into the critical region with less certainty because of the fewer terms of the series expansion which are available. Essam and Sykes assume that the high-temperature coefficients can be generated by an expression of the form of Eq. (21) which, if correct, also leads to a logarithmic dependence of the heat capacity having the limiting form

$$C/R = -0.172 \ln(1 - T_N/T) - 0.03 \quad . \tag{25}$$

Assuming this limiting dependence, the heat capacity for the entire high-temperature region can be calculated and is shown as the solid line for $T > T_N$ in Fig. 14. The agreement with the data is poor except at higher values of t, where the curve is mainly dependent on the statistically evaluated coefficients in the expansion, and thereby indicates that the limiting behavior expressed by Eq. (25) is probably incorrect.

In recent years it has been postulated that the heat capacity of three-dimensional magnetic systems with Ising-like interactions should behave, in the limit as T approaches T_N, as

$$C/R = A^{\pm} t^{-\alpha} + B^{\pm} \quad , \tag{26}$$

with $\alpha = \frac{1}{8}$ both above and below T_N. Gaunt and Domb have shown that the exact series expansion of Essam and Sykes for $T < T_N$ was not inconsistent with this hypothesis. They show that coefficients a_n in the heat-capacity expansion (6) can be represented by the expression

$$a \approx a_n' = (-1)^n 3.1 \binom{-\frac{1}{8}}{n} z_c^{-2n} \left(1 + \frac{11.2}{n}\right) \quad , \tag{27}$$

which in turn is approximated by

$$a_n' \approx a_n'' = (-1)^n 3.1 \binom{-\frac{1}{8}}{n} z_c^{-2n} + (-1)^{n+1} 39.68 \binom{\frac{7}{8}}{n} z_c^{-2n} \quad . \tag{28}$$

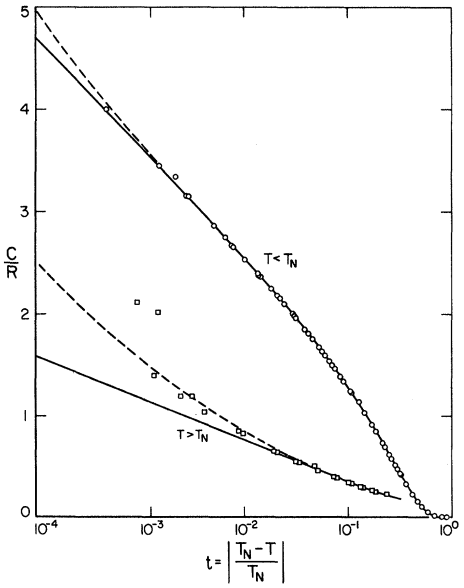

FIG. 14. Critical behavior of $DyPO_4$. The solid curves are given by the exact series expansion and have been extended to small values of t assuming a limiting logarithmic dependence [Eqs. (23) and (25)]. The dashed curves are the variation which result from assuming an exponential limiting dependence with $\alpha = \frac{1}{8}$ [Eqs. (29) and (32)].

With this expression, the heat capacity for the entire low-temperature region can be written as

$$\frac{C}{R(\ln z)} = \sum_{n=2}^{12} a_n z^{2n} = \sum_{n=0}^{12} a_n'' z^{2n} + 3.1\left(1-\frac{z^2}{z_c^2}\right)^{-1/8} - 39.68\left(1-\frac{z^2}{z_c^2}\right)^{7/8}, \tag{29}$$

which in the limit of $T \to T_N$ becomes

$$C/R = 1.6\,t^{-1/8} - 0.13 \quad . \tag{30}$$

It turns out that the heat capacity calculated by Eq. (29) is indistinguishable from that derived from Eq. (23) over the range $10^{-3} < t < 1$. At $t \simeq 10^{-3}$, C/R from Eq. (29) becomes larger than that calculated by Eq. (23), as shown by the dashed curve in Fig. 14.

With experimental values extending only slightly below $t = 10^{-3}$, one cannot choose between the two theoretical expressions, and it may not be possible to do so even with measurements extending to considerably smaller values of t. At small values of t ($t < 3\times10^{-2}$), the choice of T_N is crucial in making a meaningful fit of the data to theory. A change of 1 mK in T_N changes $\log_{10} t$ by 6% at $t = 10^{-3}$. T_N, as indicated by the heat-capacity maximum, was found by observing the rate of change of the temperature of the system as it was heated at constant rates through the transition region. At the lowest heating rate 2μW, the temperature at the position of the change in slope could be precisely determined as (3.3910 ± 0.0003) K. Even at this rate of heating, however, the thermal resistance between the sample and sample holder (250 K/W) results in a correction of − 0.0005 K, and close to T_N there may be relaxation effects of comparable magnitude in the sample itself. These considerations lead to the choice of $T_N = 3.3900$ K which was used in plotting the experimental data in Fig. 14. Unfortunately, the problem in the choice of T_N was not recognized at the time of the measurements, and curves were not taken with the sample cooling so as to bracket the true value.

Sykes, Martin, and Hunter[42] have derived an expression for the limiting form of the high-temperature heat capacity which has the $\frac{1}{8}$ power dependence and is given as

$$C/R = 1.2\,(1 - T_c/T)^{-1/8} \quad . \tag{31}$$

This expression was presumably arrived at from the behavior of high-temperature series in terms of $K = J/kT$ instead of the variable $v = \tanh K$ used in the high-temperature expansion of Essam and Sykes. If one writes the series expansion of Essam and Sykes in terms of K, one can obtain the following expression which should be approximately correct, within the assumption of Eq. (31), for all temperatures above T_N:

$$C/R = 2K^2 - 2K^4 + \frac{184}{3}K^6 - \frac{2554}{45}K^8 + 1884.394\,K^{10} - 430.836\,K^{12} + 63889.22\,K^{14} + 55759.75\,K^{16} + 1.2\left(1-\frac{K}{K_c}\right)^{-1/8} - 1.2\sum_{n=0}^{16}\left|\binom{-\frac{1}{8}}{n}\right|\left(\frac{K}{K_c}\right)^n \quad . \tag{32}$$

Equation (32) is plotted as the dashed curve for $T > T_N$ in Fig. 14. The data are in much better agreement with this expression than with Eq. (25), which has a logarithmic dependence. The large amount of scatter in the points at small values of t ($T > T_N$) indicates the difficulty in making measurements in that region.

The magnetic phase diagram for $DyPO_4$ is shown in Fig. 6. The solid circles represent the data obtained by making heat-capacity measurements between 0.75 and 4.2 K in constant magnetic fields applied along the symmetry axis. A heat-capacity curve for $DyPO_4$ in an applied field of approximately 4 KG is shown in Fig. 15. These data were obtained on the sample consisting of a large number of single crystals whose c axes had been oriented visually such that they were directed along the field direction. It should be noted that the peak is considerably broader than that obtained in zero field. The broadening is possibly due to a number of causes, such as misalignment of the c axes with respect to the magnetic field, demagnetization effects,[36,43] and the nonellipsoidal shapes of the crys-

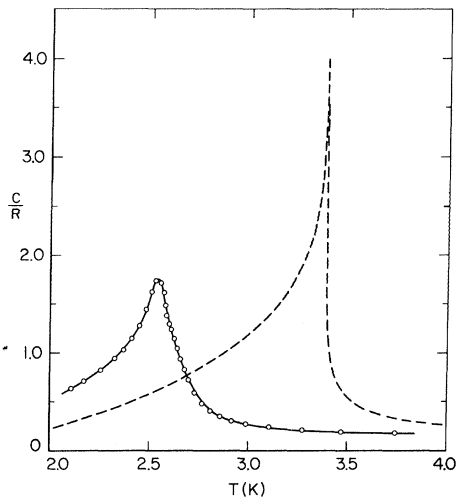

FIG. 15. Heat capacity of $DyPO_4$ in a magnetic field of 4 kG. The dashed curve represents the zero-field heat capacity.

tals. The solid circles in Fig. 6 represent the location of such peaks, obtained from a sample consisting of one single crystal in the shape of a parallelepiped, in different applied fields. The open circles represent the data obtained from spectroscopic measurements. These results have not been corrected for demagnetizing effects which are estimated to be ~ 0.5 kG at 0 K.

VI. SUMMARY AND CONCLUSIONS

This study indicates that $DyPO_4$ behaves as a very good approximation to an ideal three-dimensional Ising system. The results of heat-capacity and susceptibility measurements are in agreement with the results predicted by Essam and Sykes for the theoretical three-dimensional Ising model. The results, furthermore, are in quite good agreement with a theoretical relation between the heat capacity and the susceptibility predicted by Fisher. The results of the optical work confirm that $DyPO_4$ is a good approximation to an ideal Ising system. They indicate that the interactions are Ising-like, and that although there are significant interactions with neighbors other than the four nearest neighbors, the sum of these interactions is only about 3.4% of the four nearest-neighbor interactions.

The simplicity of the interactions and the ordered magnetic structure, the ease of crystal growth, and the relatively high ordering temperature make $DyPO_4$ a particularly attractive material for further study, especially for studies in the critical region. It shows, moreover, close agreement between theory and experiment.

ACKNOWLEDGMENT

The authors would like to express their appreciation to Dr. Calvin S. Koonce for several helpful discussions.

---

*Present address: Department of Chemistry, Purdue University, Lafayette, Ind. 47907.

†Work supported by U. S. Army Research Office, Durham, N. C.

‡National Research Council – National Bureau of Standards Postdoctoral Research Associate, 1968–1970.

[1]C. Domb, Advan. Phys. 9, 149 (1960); in *Magnetism*, edited by C. T. Rado and H. Suhl (Academic, New York, 1965), Vol. II, part A, p. 1; M. E. Fisher, Rept. Prog. Phys. 30, 615 (1967).

[2]J. W. Essam and M. F. Sykes, Physica 29, 378 (1963).

[3]M. Ball, M. T. Hutchings, M. J. M. Leask, and W. P. Wolf, in *Proceedings of the Eighth International Conference on Low-Temperature Physics* (Butterworths, London, 1963), p. 248.

[4]M. J. M. Leask, J. Appl. Phys. 39, 908 (1968).

[5]S. Hüfner, M. Schinkmann, and H. Schmidt, Phys. Kondensierten Materie 4, 108 (1965).

[6]H. Schuchert, S. Hüfner, and R. Faulhaber, J. Appl. Phys. 39, 1137 (1968).

[7]G. A. Prinz, Phys. Letters 20, 323 (1966).

[8]G. T. Rado, Phys. Rev. Letters 23, 644 (1969).

[9]B. Schneider, D. P. Landau, B. E. Keen, and W. P. Wolf, Phys. Letters 23, 210 (1966).

[10]A. H. Cooke, K. A. Gehring, M. J. M. Leask, D. D. Smith, and J. H. M. Thornley, Phys. Rev. Letters 14, 685 (1965).

[11]B. E. Keen, D. Landau, B. Schneider, and W. P. Wolf, J. Appl. Phys. 37, 1120 (1966).

[12]P. D. Scott and W. P. Wolf, J. Appl. Phys. 40, 1031 (1969).

[13]S. Hüfner, L. Holmes, F. Varsanyi, and L. G. Van Uitert, Phys. Rev. 171, 507 (1968).

[14]R. F. Wielirga, H. W. J. Blöte, J. A. Roest, and W. J. Huiskamp, Physica 34, 223 (1967).

[15]K. W. Mess, E. Lagendijk, D. A. Curtis, and W. J. Huiskamp, Physica 34, 126 (1967).

[16]H. W. J. Blöte and W. J. Huiskamp, Phys. Letters 29A, 304 (1969).

[17]S. de S. Barros and S. A. Friedberg, Phys. Rev. 141, 637 (1966).

[18]R. Bidaux and P. Meriel, J. Phys. (Paris) 29, 357 (1968).

[19]J. H. Colwell, B. W. Mangum, D. D. Thornton, J. C. Wright, and H. W. Moos, Phys. Rev. Letters 23, 1245 (1969).

[20]R. W. G. Wyckoff, *Crystal Structures*, 2nd ed. (Interscience, New York, 1965), Chap. VIII.

[21]R. S. Feigelson, J. Am. Ceram. Soc. 47, 257 (1964).

[22]J. H. Colwell, Rev. Sci. Instr. 40, 1182 (1969).

[23]H. Plumb and G. Cataland, Metrologia 2, 127 (1956).

[24]R. H. Sherman, S. G. Sydoriak, and T. R. Roberts, J. Res. Natl. Bur. Std. A68, 579 (1964); F. G. Brickwedde, H. Van Dijk, M. Durieux, J. R. Clement, and J. K. Logan, Natl. Bur. Std. (U.S.) Monograph No. 10 (1960).

[25]C. R. Barber and A. Horsford, Brit. J. Appl. Phys. 14, 920 (1963).

[26]M. F. Sykes, J. W. Essam, and D. S. Gaunt, J. Math. Phys. 6, 283 (1965).

[27]D. S. Gaunt and C. Domb, J. Phys. C 1, 1038 (1968).

[28]S. Yatsiv, Physica 28, 521 (1962).

[29]B. G. Wybourne, J. Chem. Phys. 36, 2310 (1962).

[30]Peter M. Levy, Phys. Rev. 177, 509 (1969).

[31]J. M. Ziman, Proc. Phys. Soc. (London) 64, 1108 (1951).

[32]For further details, see J. C. Wright, Ph.D. dissertation, The Johns Hopkins University, 1970 (unpublished), available from University Microfilms, Inc., Ann Arbor, Mich.

[33]M. Ball, W. P. Wolf, and A. F. G. Wyatt, Phys. Letters 10, 7 (1964).

[34]A. H. Cooke and J. G. Park, Proc. Phys. Soc. (London) A69, 282 (1956).

[35]J. G. Park, Proc. Roy. Soc. (London) A245, 118 (1958).

[36]Peter M. Levy, Phys. Rev. 170, 595 (1968).

[37]M. E. Fisher, Phil. Mag. 7, 1731 (1962).

[38]W. P. Wolf and A. F. G. Wyatt, Phys. Rev. Letters 13, 368 (1964).

[39]J. Skalyo, Jr., A. F. Cohen, S. A. Friedberg, and Robert B. Griffiths, Phys. Rev. 164, 705 (1967).

[40]M. F. Sykes and M. E. Fisher, Phys. Rev. Letters

1, 321 (1958).
[41]G. A. Prinz (private communication).
[42]M. F. Sykes, J. L. Martin, and D. L. Hunter, Proc. Phys. Soc. (London) 91, 671 (1967).
[43]P. M. Levy and D. P. Landau, J. Appl. Phys. 39, 1128 (1968).

PHYSICAL REVIEW B VOLUME 3, NUMBER 3 1 FEBRUARY 1971

Mössbauer Study of the Ferroelectric Phase Transition in Potassium Ferrocyanide Trihydrate

P. A. Montano and H. Shechter
Physics, Technion-Israel Institute of Technology, Haifa, Israel
and
U. Shimony
Electrical Engineering, Technion-Israel Institute of Technology, Haifa, Israel
(Received 19 May 1970)

An increase in the area of the Mössbauer spectrum at the ferroelectric transition point has been observed in single crystals of potassium ferrocyanide trihydrate (KFCT), for spectra with the γ beam in a direction near the ferroelectric $[10\bar{1}]$ axis. Also an anomalous change in the center shift appears at the transition point. This behavior is related to polarization effects, due to the presence of small quadrupole splitting in KFCT and to changes in the orientation of the electric field gradient caused by the onset of ferroelectricity.

I. INTRODUCTION

Recently, contradictory results have been reported on the behavior of the Mössbauer recoiless fraction in $K_4Fe(CN)_6 \cdot 3H_2O$ (KFCT), near the ferroelectric transition. Hazony *et al.*[1] measured the Mössbauer spectral area on single crystals of KFCT and found an anomalous increase related to the f factor near T_c, when the observation direction was close to the ferroelectric axis. Gleason and Walker[2] and Clauser[3] do not observe any changes in the spectral area of powder samples at the transition temperature. We measured the Mössbauer spectral area of KFCT single crystals in a direction close to $[10\bar{1}]$ (ferroelectric axis) and [010] directions and results similar to those of Hazony *et al.* were obtained; the anomalies are related to polarization effects that may average in powders.

The KFCT crystallizes from a water solution.[4] The water molecules are located in layers perpendicular to the [010] axis. Between each layer of water there are two layers of $Fe(CN)_6^{-4}$ groups and interspersed potassium ions, with the iron nuclei located at the center of a regular octahedra formed by cyanide ions.[5,6] The basic structure is either tetragonal, which is metastable at room temperature (rt) or monoclinic, which is pseudotetragonal ($\beta = 90 \pm 3$) and stable at rt. Under practical conditions of crystal growth, complex lamellar twin crystals and polytypic structures often appear, in which monoclinic and tetragonal layers alternate in a microscopic scale.[6,7] The tetragonal modification of KFCT is changed irreversibly into the ferroelectric monoclinic at 218 °K. The monoclinic structure of KFCT shows a spontaneous polarization below 248 °K in the $[10\bar{1}]$ direction.[8,9] The phase transition at 248 °K is accompanied by a change in the crystal symmetry, $C_{2/c}$ to C_c. Anomalies have been observed in the sound velocity in KFCT in the $[10\bar{1}]$ and [101] directions at the transition point.[10] Recently, the ferroelectric transition in KFCT has been investigated under hydrostatic pressure[11] suggesting that the KFCT is a hard ferroelectric with a second-order transition.

It has been suggested that ferroelectricity in KFCT is of the water molecule order-disorder type.[12] A simple order-disorder model of O'Reilly and Schacher[13] explains qualitatively the behavior of the spontaneous polarization in KFCT. However, contribution to the spontaneous polarization and internal field due to displacement and, polarizability of the K^+ and $Fe(CN)_6^{-4}$ have to be considered as well, since there is experimental evidence that the movement of the water molecules shows no anomalies at the ferroelectric transition.[14,15]

II. EXPERIMENTAL PROCEDURE

The samples were selected from grown single crystals of $K_4Fe(CN)_6 \cdot 3H_2O$. These yielded a Laue pattern with a twofold symmetry, when observed perpendicular to the [010] plane. The polarization axis was identified through capacity measurements. The crystal was found to have a polytypic structure of a monoclinic crystal with microscopic layers of tetragonal stacks[6,7] and dielectric transitions at 248.5 and 230 °K. These transition points were